Adaptive Control of Harmonic Drives Based on Virtual Decomposition

Wen-Hong Zhu, *Senior Member, IEEE*, Erick Dupuis, Michel Doyon, and Jean-Claude Piedboeuf

***Abstract*—Harmonic drives are interesting for robotic applications due to their attractive properties such as high reduction ratio, compact size, low mass, and coaxial assembly. However, the high friction and the dynamics of the flexspline are the main issues that significantly challenge the control systems. In this paper, an adaptive controller capable of adaptively compensating the friction, while incorporating the dynamics of the flexspline, is developed in both joint torque and joint-position control modes. The *virtual decomposition control* approach allows the dynamics of harmonic drives to be controlled separately from the conventional dynamics of the robots. Adaptive friction compensation and flexspline dynamics based control are the two main contributions of this paper. The L_2/L_∞ stability and the L_2-gain-induced H_∞ stability are guaranteed. Experimental results demonstrated in both time and frequency domains confirm the feasibility of the proposed approach.**

***Index Terms*—Adaptive control, harmonic drives, motion control, precision control systems, torque control, virtual decomposition control.**

I. Introduction

HARMONIC drives have received increasing attention in robotic applications due to their attractive properties such as high reduction ratio, compact size, light weight, and coaxial assembly. For controlling a robot manipulator with harmonic drives, one needs to address not only the conventional dynamics of the robot, but also the specific dynamics of the harmonic drives [1]–[3], in view of the *virtual decomposition control* [4], [5].

There exist distinguishable factors particularly associated with the dynamics of harmonic drives, such as friction, dynamics of the flexspline, nonlinearity, hysteresis, and so on [3], [6]–[8]. In this paper, four different types of harmonic drives from HD Systems Inc. are examined, and the high friction and the dynamics of the flexspline are identified as two main dynamics issues that will be addressed in the control design.

Control of harmonic drives can be classified into two categories. The first category is the input–output based control [9], [10]. The approaches in this category model the harmonic drive as a linear input–output block and apply H_∞ control and μ-synthesis. As a result, the derived controllers are quite sensitive to operational conditions. In [10], two controllers, derived for the constrained motion and for the free motion, demonstrated a difference in parameters that is more than an order of magnitude. The second category is the model-based control. The dynamics of the flexspline is modeled as a pure torsional spring [11] such that the control technology developed for flexible-joint robots [12] can be applied. Due to the approximation in modeling, dynamic uncertainties of harmonic drives always exist, which may complicate the parameter identification procedure and may even result in a big bias in parameter estimation. Therefore, using adaptive control to automatically handle the parameter uncertainties is motivated.

In this paper, an adaptive controller capable of adaptively compensating the friction, while incorporating the dynamics of the flexspline, is developed in both joint torque and joint position control modes. This turns out to be of great importance due to the significant and somewhat uncertain characteristics of the friction inherent to the four types of harmonic drives from HD Systems Inc. The *virtual decomposition control* approach allows the adaptive controller designed for harmonic drives to be efficiently integrated into the adaptive controller designed for rigid-link robots by simply incorporating a joint velocity error term into the control law to form appropriate *virtual power flows*. In the controller, torque measurement from strain gauges mounted on the flexspline [13]–[16] is used, in addition to the joint position measurement from a resolver and the motor rotor position measurement from an encoder. In the torque control mode, the position and velocity errors of the motor rotor and the joint torque error are L_2 and L_∞ stable. In the position control mode, the position and velocity errors of both the joint and the motor rotor and the joint torque error are L_2 and L_∞ stable. Based on the equivalence between the L_2 stability and the H_∞ stability [17], [18], the L_2-gain-induced H_∞ stability is guaranteed for all the variables that possess the L_2 stability. The conditions of achieving asymptotic stability are discussed. Extensive experimental results demonstrated in both time domain and frequency domain confirm the feasibility of the proposed approach. The effectiveness of the friction compensation and of the flexspline-dynamics-based control is presented. The advantage of using adaptive friction compensation over fixed-parameter friction compensation is demonstrated. A substantial improvement in position-tracking control (about four times) over a PID controller is also achieved. The proposed adaptive joint controller for harmonic drives can be easily incorporated into most motion/force controllers previously designed for robot manipulators, based on either the torque-control interface or on the virtual decomposition control approach.

This paper is organized as follows. Section II presents the model of harmonic drives by taking into account the friction

Manuscript received February 26, 2004; revised June 24, 2005. Recommended by Technical Editor B. Yao.

W.-H. Zhu, E. Dupuis, and M. Doyon are with the Canadian Space Agency, Saint-Hubert, QC J3Y 8Y9, Canada (e-mail: wen-hong.zhu@space.gc.ca; erick.dupuis@space.gc.ca; michel.doyon@space.gc.ca).

J.-C. Piedboeuf is with the Canadian Space Agency, Saint-Hubert, QC J3Y 8Y9, Canada, and with the University of Waterloo, Waterloo, ON N2L 3G1, Canada, and also with Ecole Polytechnique, Montreal, QC H3C 3A7, Canada (e-mail: jean-claude.piedboeuf@space.gc.ca).

Digital Object Identifier 10.1109/TMECH.2006.882992

and the flexspline dynamics. Section III presents adaptive control and analysis. Section IV presents the experimental results achieved on several commercially available harmonic drives.

II. Harmonic Drive Dynamics

There have been extensive studies on modeling of harmonic drives [6], [7]. A typical harmonic drive consists of a wave generator that is connected to the motor, a circular spline that is connected to the base, and a flexspline that is placed in between and connected to the joint. The flexspline is a deformable device and, in this paper, is modeled as a pure torsional spring with a damping effect by ignoring vibration modes caused by mass distribution.

The dynamic equation of a harmonic drive assembled with a dc motor can be written as

$$k_{\rm f}[d(\dot{\phi}-\dot{q})+(\phi-q)]=\tau \tag{1}$$

$$I^*\ddot{\phi}+f_\phi(\dot{\phi},\tau)+k_{\rm f}[d(\dot{\phi}-\dot{q})+(\phi-q)]=u+u_{\rm d} \tag{2}$$

where τ is the physical torque passing through the flexspline, $k_{\rm f}>0$ is the stiffness of the flexspline, ϕ is the angle of the motor rotor divided by the gear ratio, q is the joint angle; $k_{\rm f}d>0$ is the damping coefficient of the flexspline, I^* is the rotor inertia of the dc motor multiplied by the gear ratio squared, $f_\phi(\dot{\phi},\tau)$ is the frictional torque that is assumed to be a function of the motor rotor velocity and the payload, u is the motor driving torque multiplied by the gear ratio, and $u_{\rm d}\in L_\infty$ is the disturbance torque caused by external disturbances.

Remark 2.1: Introducing damping effect into the flexspline dynamics can be found in [19], and recently in [20]. In case of $d=0$, (1) and (2) are equivalent to the dynamics of a flexible joint [5], [12], [21].

The model of the frictional torque $f_\phi(\dot{\phi},\tau)$ takes the Coulomb and viscous effects into account, and is expressed as

$$f_\phi(\dot{\phi},\tau)=\begin{cases} g(\tau)k_{\rm c}+c+k_{\rm vp}\dot{\phi}, & \dot{\phi}>0\\ [-g(\tau)k_{\rm c},g(\tau)k_{\rm c}]+c, & \dot{\phi}=0\\ -g(\tau)k_{\rm c}+c+k_{\rm vn}\dot{\phi}, & \dot{\phi}<0\end{cases}$$

$$\stackrel{\rm def}{=}Y_\phi(\dot{\phi},\tau)\theta \tag{3}$$

where $k_{\rm c}>0$ is the magnitude of the Coulomb torque at zero payload and $c>0$ is a dc offset. Introducing the dc offset c in the friction model allows the Coulomb friction to have different values at positive and negative velocities, $k_{\rm vp}>0$ and $k_{\rm vn}>0$ are the viscous friction coefficients at positive and negative velocities, respectively

$$g(t)\stackrel{\rm def}{=}1+g_1\mid\tau\mid+g_2\mid\tau\mid^2 \tag{4}$$

with $g_1>0$ and $g_2>0$, is a function used to emulate the load-dependent Coulomb friction effect, and

$$\theta=[\,k_{\rm c}\quad c\,k_{\rm vp}\quad k_{\rm vn}\,]^T\in R^4$$

represents the uncertain parameter vector and $Y_\phi(\dot{\phi},\tau)\in R^{1\times 4}$ represents the corresponding regressor matrix.

Remark 2.2: In this paper, the payload-dependent friction is modeled as a quadratic form instead of a linear form [19] to better preserve the nature of the problem. Fig. 1 shows the magnitude of the Coulomb friction versus the payload with respect to a special harmonic drive CSF-45-120-2A-GR from HD Systems Inc. It is clearly shown that the quadratic fitting is much more accurate than the linear fitting. It is also worth noting that the payload-dependent friction is very significant. The Coulomb friction of the harmonic drive CSF-45-120-2A-GR at a 1000-N·m payload is almost about seven to eight times higher than that without the payload.

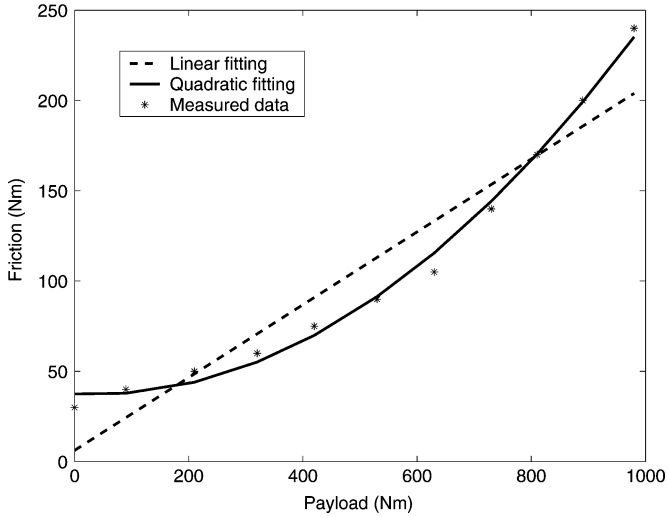

Fig. 1. Payload-dependent Coulomb friction of the harmonic drive CSF-45-120-2A-GR.

III. Adaptive Control and Analysis

A. Adaptive-Control Algorithms

The adaptive control has been used to compensate for the friction due to the nature of the friction that is significant and somewhat uncertain. In [5], an adaptive-control law proposed for controlling the flexible-joint robots is able to achieve asymptotic stability of the position-tracking control for both the joints and the motor rotors. However, no torque control is ensured due to the fact that the estimate of the flexspline stiffness will not generally converge to the true value. In order to achieve the torque control in addition to the motion control, a new control algorithm that uses direct torque measurement, is proposed as follows:

$$F(s)\stackrel{\rm def}{=}\frac{1}{ds+1} \tag{5}$$

$$\zeta\stackrel{\rm def}{=}\frac{1}{k_{\rm f}} \tag{6}$$

$$\phi_{\rm d}=q+F(s)\hat{\zeta}\tau_{\rm r} \tag{7}$$

$$\dot{\phi}_{\rm r}=\dot{\phi}_{\rm d}+\lambda_{\rm q}(\dot{q}_{\rm r}-\dot{q})+\lambda_\phi(\phi_{\rm d}-\phi)+\lambda_\tau(\tau_{\rm r}-\tau) \tag{8}$$

$$u=I^*\ddot{\phi}_{\rm r}+\hat{f}_\phi(\dot{\phi}_{\rm r},\tau)+k_\phi(\dot{\phi}_{\rm r}-\dot{\phi})+\tau_{\rm r}+k_\tau(\tau_{\rm r}-\tau) \tag{9}$$

where $\tau_{\rm r}$ representing the required torque will be designed in the motion controller, $\hat{\zeta}$ is the estimate of ζ defined by (6); $\dot{q}_{\rm r}$ is the required joint velocity; $\lambda_{\rm q}>0,\lambda_\phi>0,\lambda_\tau>0,k_\phi>0,$

TABLE I
HARMONIC DRIVES AND MOTOR PARAMETERS

	Motor	Harmonic drive	Gear ratio	Stiffness (Nm/rad)
Joint 3	RBEH-3002	CSF-45-120-2A-GR	120	2.9×10^5
Joint 4	RBEH-2103	CSF-32-120-2A-GR	120	1.1×10^5
Joint 5	RBEH-1503	CSF-25-160-2A-GR	160	5.0×10^4
Joint 7	RBEH-1503	CSF-20-160-2A-GR	160	2.6×10^4

and $k_\tau > 0$ are the control gains; and

$$\hat{f}_\phi(\dot{\phi}_\mathrm{r}, \tau) = Y_\phi(\dot{\phi}_\mathrm{r}, \tau)\hat{\theta}. \tag{10}$$

Equation (5) defines a low-pass filter and (6) defines a new parameter ζ. Equation (7) forms the desired motor-rotor-position ϕ_d, and (8) forms the required rotor velocity in which the torque error is added. Finally, (9) presents the control law that consists of the flexspline-dynamics-based feedforward compensation and feedback control.

The parameter estimates $\hat{\theta}$ and $\hat{\zeta}$ are updated in real-time by using the $\mathcal{P}$ function defined in [5, p. 311] as

$$\hat{\theta}_i = \mathcal{P}(s_i(t), \rho_i, \theta_i^-, \theta_i^+) \tag{11}$$

$$\hat{\zeta} = \mathcal{P}(s_\zeta(t), \rho_\zeta, \zeta^-, \zeta^+) \tag{12}$$

where $\hat{\theta}_i$ is the ith element of $\hat{\theta}$, $i = 1, 2, 3, 4$; $\rho_i > 0$ is an update gain; θ_i^- and θ_i^+ are the lower and upper bounds of the ith element of θ; and $s_i(t)$ is the ith element of $s(t) \in R^4$ defined by

$$s(t) \triangleq (\dot{\phi}_\mathrm{r} - \dot{\phi}) Y_\phi(\dot{\phi}_\mathrm{r}, \tau)^T. \tag{13}$$

Accordingly, $\rho_\zeta > 0$ is an update gain, ζ^- and ζ^+ are the lower and upper bounds of ζ, and $s_\zeta(t)$ is governed by

$$s_\zeta(t) = -(1 + k_\tau)\tau_\mathrm{r} \left[(\dot{\phi}_\mathrm{d} - \dot{\phi}) + \lambda_\phi(\phi_\mathrm{d} - \phi) \right]. \tag{14}$$

Remark 3.1: The control laws defined by (5)–(9) have a few differences from the control laws previously proposed for controlling the flexible-joint robots [5]. First, the actual joint position q instead of the desired joint position is measured and used directly for deriving the joint torque control—a function that does not exist in [5]. Second, the joint torque is directly measured and used in forming both the required motor velocity $\dot{\phi}_\mathrm{r}$ and the control torque u.

Remark 3.2: In view of (8) and (9), $\ddot{\phi}_\mathrm{r}$ in u is a linear function of $\dot{\tau}$, and so is u. However, $\ddot{\phi}$ is a linear function of u in view of (2), and $\dot{\tau}$ is a linear function of $\ddot{\phi}$ in view of (1). Thus, an algebraic loop involving $\dot{\tau}, \ddot{\phi}_\mathrm{r}, u$, and $\ddot{\phi}$ is formed in view of (1), (2), (8), and (9). A necessary and sufficient condition to ensure the stability of this algebraic loop in discrete-time implementation is $k_\mathrm{f} d \lambda_\tau < 1$, which imposes a limitation on the torque feedback gain λ_τ in (8). The parameters listed in Tables I and II yield $\max\{k_\mathrm{f} d \lambda_\tau\} = 0.058 < 1$.

Remark 3.3: In view of (5)–(9), the variables required for implementing the control torque u include the joint position q, the velocity $\dot{q}$, and the acceleration $\ddot{q}$; the motor position ϕ and velocity $\dot{\phi}$; the joint torque τ and its derivative $\dot{\tau}$. As will be shown later, τ_r and $\dot{\tau}_\mathrm{r}$ are functions of the referenced signals and of the positions, velocities, and accelerations of the entire robot.

TABLE II
CONTROL PARAMETERS

	Joint 3	Joint 4	Joint 5	Joint 7
$d\ (s)$	0.001	0.001	0.001	0.001
λ_q	0.3	0.35	0.3	0.1
$\lambda_\phi\ (1/s)$	50	45	50	50
$\lambda_\tau\ (1/Nms)$	0.0002	0.0002	0.0002	0.0002
$I^*\ (Nms^2)$	28*	5	2.1	1.0
$k_\phi\ (Nms)$	500	200	100	25
k_τ	0	0.8	0.75	1.0
$\rho_1\ (Nm)$	2000	2000	1000	400
$\theta_1^-\ (Nm)$	-35	-5	-4	-4
$\theta_1^+\ (Nm)$	35	5	4	7
$\rho_2\ (Nm)$	10000	200	100	100
$\theta_2^-\ (Nm)$	-200	-50	-20	-10
$\theta_2^+\ (Nm)$	200	50	20	10
$\rho_3\ (Nms^2)$	50000	30000	50000	40000
$\theta_3^-\ (Nms)$	0	0	0	0
$\theta_3^+\ (Nms)$	700	90	90	80
$\rho_4\ (Nms^2)$	50000	30000	50000	40000
$\theta_4^-\ (Nms)$	0	0	0	0
$\theta_4^+\ (Nms)$	700	90	90	80
$\rho_\zeta\ (1/(Nm)^2)$	1.0×10^{-6}	1.0×10^{-5}	1.0×10^{-4}	1.0×10^{-4}
$\zeta^-\ (1/Nm)$	2.5×10^{-6}	7×10^{-6}	1.5×10^{-5}	3.0×10^{-5}
$\zeta^+\ (1/Nm)$	3.5×10^{-6}	1.0×10^{-5}	2.5×10^{-5}	4.0×10^{-5}
$k_p\ (Nms)$	2000	500	100	80
$k_I\ (Nm)$	25000	4000	2000	2000
$t_s^-\ (Nm)$	-400	-200	-100	-50
$t_s^+\ (Nm)$	400	200	100	50
$\lambda\ (1/s)$	25	45	30	30

* The value used in the controller may be different from the physical value.

The following inequalities hold:

$$(\dot{\phi}_\mathrm{r} - \dot{\phi}) \left[Y_\phi(\dot{\phi}, \tau) - Y_\phi(\dot{\phi}_\mathrm{r}, \tau) \right] \theta \le 0 \tag{15}$$

$$\begin{aligned} &(\dot{\phi}_\mathrm{r} - \dot{\phi}) Y_\phi(\dot{\phi}_\mathrm{r}, \tau)(\theta - \hat{\theta}) - \sum_{i=1}^{4} \left[(\theta_i - \hat{\theta}_i) \frac{\dot{\hat{\theta}}_i}{\rho_i} \right] \\ &\quad = \sum_{i=1}^{4} \left\{ (\theta_i - \hat{\theta}_i) \left[s_i(t) - \frac{\dot{\hat{\theta}}_i}{\rho_i} \right] \right\} \le 0 \end{aligned} \tag{16}$$

$$\begin{aligned} &-(1 + k_\tau)\tau_\mathrm{r} \left[(\dot{\phi}_\mathrm{d} - \dot{\phi}) + \lambda_\phi(\phi_\mathrm{d} - \phi) \right] (\zeta - \hat{\zeta}) - (\zeta - \hat{\zeta}) \dot{\hat{\zeta}} / \rho_\zeta \\ &\quad = (\zeta - \hat{\zeta}) \left[s_\zeta(t) - \dot{\hat{\zeta}} / \rho_\zeta \right] \le 0. \end{aligned} \tag{17}$$

The first inequality is from the definition of Y_ϕ in (3), and the second and the third inequalities are from [5, Lemma 1, p. 311].

Substituting (9) into (2) and using (1), (3), and (10) yields

$$\begin{aligned} I^*(\ddot{\phi}_\mathrm{r} - \ddot{\phi}) &= -k_\phi(\dot{\phi}_\mathrm{r} - \dot{\phi}) \\ &\quad + f_\phi(\dot{\phi}, \tau) - \hat{f}_\phi(\dot{\phi}_\mathrm{r}, \tau) \\ &\quad - (\tau_\mathrm{r} - \tau) - k_\tau(\tau_\mathrm{r} - \tau) - u_\mathrm{d} \\ &= -k_\phi(\dot{\phi}_\mathrm{r} - \dot{\phi}) \\ &\quad - (1 + k_\tau)(\tau_\mathrm{r} - \tau) - u_\mathrm{d} \\ &\quad + [Y_\phi(\dot{\phi}, \tau)\theta - Y_\phi(\dot{\phi}_\mathrm{r}, \tau)\theta] \\ &\quad + Y_\phi(\dot{\phi}_\mathrm{r}, \tau)\theta - Y_\phi(\dot{\phi}_\mathrm{r}, \tau)\hat{\theta}. \end{aligned} \tag{18}$$

In view of (1) and (5)–(7), it follows that

$$\tau_{\rm r} - \tau = k_{\rm f}[d(\dot{\phi}_{\rm d} - \dot{\phi}) + (\phi_{\rm d} - \phi) + (\zeta - \hat{\zeta})\tau_{\rm r}]. \tag{19}$$

A nonnegative function is defined as

$$V_1 = \frac{1}{2}\left[I^*(\dot{\phi}_{\rm r} - \dot{\phi})^2 + k_{\rm f}(1+k_\tau)(1+\lambda_\phi d)(\phi_{\rm d} - \phi)^2 + \sum_{i=1}^{4}\frac{(\theta_i - \hat{\theta}_i)^2}{\rho_i} + \frac{k_{\rm f}(\zeta - \hat{\zeta})^2}{\rho_\zeta}\right]. \tag{20}$$

Differentiating (20) with respect to time and applying (15)–(19) and (8) into it yield

$$\begin{aligned}
\dot{V}_1 &= (\dot{\phi}_{\rm r} - \dot{\phi})I^*(\ddot{\phi}_{\rm r} - \ddot{\phi}) - \sum_{i=1}^{4}(\theta_i - \hat{\theta}_i)\frac{\dot{\hat{\theta}}_i}{\rho_i} - \frac{k_{\rm f}(\zeta - \hat{\zeta})\dot{\hat{\zeta}}}{\rho_\zeta} \\
&\quad + k_{\rm f}(1+k_\tau)(1+\lambda_\phi d)(\phi_{\rm d} - \phi)(\dot{\phi}_{\rm d} - \dot{\phi}) \\
&\le -k_\phi(\dot{\phi}_{\rm r} - \dot{\phi})^2 - (\dot{\phi}_{\rm r} - \dot{\phi})u_{\rm d} - (1+k_\tau)(\dot{\phi}_{\rm r} - \dot{\phi})(\tau_{\rm r} - \tau) \\
&\quad - \frac{k_{\rm f}(\zeta - \hat{\zeta})\dot{\hat{\zeta}}}{\rho_\zeta} + k_{\rm f}(1+k_\tau)(1+\lambda_\phi d)(\phi_{\rm d} - \phi)(\dot{\phi}_{\rm d} - \dot{\phi}) \\
&\le -\left[k_\phi - \left(\frac{1}{2\gamma}\right)^2\right](\dot{\phi}_{\rm r} - \dot{\phi})^2 + (\gamma u_{\rm d})^2 \\
&\quad - \frac{k_{\rm f}(\zeta - \hat{\zeta})\dot{\hat{\zeta}}}{\rho_\zeta} - (1+k_\tau)(\dot{\phi}_{\rm r} - \dot{\phi})(\tau_{\rm r} - \tau) \\
&\quad + k_{\rm f}(1+k_\tau)(1+\lambda_\phi d)(\phi_{\rm d} - \phi)(\dot{\phi}_{\rm d} - \dot{\phi}) \\
&\le -\left[k_\phi - \left(\frac{1}{2\gamma}\right)^2\right](\dot{\phi}_{\rm r} - \dot{\phi})^2 + (\gamma u_{\rm d})^2 \\
&\quad - (1+k_\tau)\lambda_{\rm q}(\dot{q}_{\rm r} - \dot{q})(\tau_{\rm r} - \tau) \\
&\quad - (1+k_\tau)\lambda_\tau(\tau_{\rm r} - \tau)^2 - (1+k_\tau)[\dot{\phi}_{\rm d} - \dot{\phi} + \lambda_\phi(\phi_{\rm d} - \phi)] \\
&\quad \times \{k_{\rm f}[d(\dot{\phi}_{\rm d} - \dot{\phi}) + (\phi_{\rm d} - \phi)]\} \\
&\quad + k_{\rm f}(1+k_\tau)(1+\lambda_\phi d)(\phi_{\rm d} - \phi)(\dot{\phi}_{\rm d} - \dot{\phi}) \\
&= -\left[k_\phi - \left(\frac{1}{2\gamma}\right)^2\right](\dot{\phi}_{\rm r} - \dot{\phi})^2 - (1+k_\tau)k_{\rm f}d(\dot{\phi}_{\rm d} - \dot{\phi})^2 \\
&\quad - (1+k_\tau)k_{\rm f}\lambda_\phi(\phi_{\rm d} - \phi)^2 \\
&\quad - (1+k_\tau)\lambda_\tau(\tau_{\rm r} - \tau)^2 + (\gamma u_{\rm d})^2 \\
&\quad - (1+k_\tau)\lambda_{\rm q}(\dot{q}_{\rm r} - \dot{q})(\tau_{\rm r} - \tau)
\end{aligned} \tag{21}$$

where $\gamma > 0$ is a constant subject to

$$k_\phi - \left(\frac{1}{2\gamma}\right)^2 > 0. \tag{22}$$

The controller described by (5)–(14) is able to provide either a torque-control interface or an inner kernel for the position control. The following analysis will address it in detail.

B. Joint Torque Control

In the torque control mode, $\tau_{\rm r} \in L_\infty$ and $\dot{\tau}_{\rm r} \in L_\infty$ are assumed, and $\lambda_{\rm q} = 0$ is used. By specifying $\gamma^2 = \frac{1}{2k_\phi}$, integrating (21) over time from $t = 0$ to $t = T$, $\forall\, T > 0$, yields

$$\int_0^T (\dot{\phi}_{\rm r} - \dot{\phi})^2 dt \le \frac{1}{k_\phi^2}\int_0^T u_{\rm d}^2 dt + \frac{2}{k_\phi}V_1(0) \tag{23}$$

$$\int_0^T (\phi_{\rm d} - \phi)^2 dt \le \frac{1}{2k_\phi(1+k_\tau)\lambda_\phi k_{\rm f}}\int_0^T u_{\rm d}^2 dt + \frac{1}{(1+k_\tau)\lambda_\phi k_{\rm f}}V_1(0) \tag{24}$$

$$\int_0^T (\dot{\phi}_{\rm d} - \dot{\phi})^2 dt \le \frac{1}{2k_\phi(1+k_\tau)dk_{\rm f}}\int_0^T u_{\rm d}^2 dt + \frac{1}{(1+k_\tau)dk_{\rm f}}V_1(0) \tag{25}$$

$$\int_0^T (\tau_{\rm r} - \tau)^2 dt \le \frac{1}{2k_\phi(1+k_\tau)\lambda_\tau}\int_0^T u_{\rm d}^2 dt + \frac{1}{(1+k_\tau)\lambda_\tau}V_1(0). \tag{26}$$

Equations (23)–(26) guarantee the L_2 stability of the mapping from $u_{\rm d}$ to $\dot{\phi}_{\rm r} - \dot{\phi}, \phi_{\rm d} - \phi, \dot{\phi}_{\rm d} - \dot{\phi}$, and $\tau_{\rm r} - \tau$ [17, pp. 262-264]. In case of $V_1(0) = 0$, it further guarantees the L_2-gain-induced H_∞ stability [18].

Lemma 1: Consider a nonnegative piecewise continuous function $\xi(t)$ defined as

$$\xi(t) = X^T P X + \alpha(t)$$

with $X \in \Re^n$ and $P \in \Re^{n\times n}$ being a positive-definite symmetric matrix, $\alpha(t) \ge 0$, and $\alpha(t) \in L_\infty$. If the time derivative of $\xi(t)$ is governed by

$$\dot{\xi}(t) \le -X^T Q X + \beta(t)$$

with $Q \in \Re^{n\times n}$ being a positive-definite symmetric matrix, and $\beta(t) \in L_\infty$, then it follows that

$$\xi(t) \in L_\infty \text{ and } X \in L_\infty^n.$$

Proof: In view of $\alpha(t) \in L_\infty$ and $\beta(t) \in L_\infty$, there exist

$$|\,\alpha(t)\,| \le c_\alpha < \infty$$
$$|\,\beta(t)\,| \le c_\beta < \infty.$$

Let $b^- = \lambda_{\min}(Q)$ and $a^+ = \lambda_{\max}(P)$. It follows that $\dot{\xi}(t) \le 0$, when $\xi(t) \ge \frac{a^+}{b^-}c_\beta + c_\alpha$. Thus,

$$|\,\xi(t)\,| \le \max\left\{|\,\xi(0)\,|, \frac{a^+}{b^-}c_\beta + c_\alpha\right\}, \qquad \forall t$$

becomes valid.

In view of Lemma 1, (20) and (21) with $\lambda_{\rm q} = 0$, and $u_{\rm d} \in L_\infty$, the L_∞ stability for $\dot{\phi}_{\rm r} - \dot{\phi}$ and $\phi_{\rm d} - \phi$ can be ensured. In view

of (8) and (19), it yields

$$\begin{bmatrix} 1 & \lambda_\tau \\ -k_{\rm f}d & 1 \end{bmatrix} \begin{bmatrix} \dot{\phi}_{\rm d}-\dot{\phi} \\ \tau_{\rm r}-\tau \end{bmatrix} = \begin{bmatrix} \dot{\phi}_{\rm r}-\dot{\phi}-\lambda_\phi(\phi_{\rm d}-\phi) \\ k_{\rm f}(\phi_{\rm d}-\phi)+k_{\rm f}\tau_{\rm r}(\zeta-\hat{\zeta}) \end{bmatrix}. \tag{27}$$

Since $\dot{\phi}_{\rm r}-\dot{\phi}\in L_\infty, \phi_{\rm d}-\phi\in L_\infty$, and $\tau_{\rm r}\in L_\infty$, the term on the right-hand side of (27) is bounded. Note that the 2×2 matrix on the left-hand side of (27) is of full rank. Therefore, $\dot{\phi}_{\rm d}-\dot{\phi}\in L_\infty$ and $\tau_{\rm r}-\tau\in L_\infty$ can be ensured. If $u_{\rm d}\in L_2$, it follows from (23)–(26) that

$$\dot{\phi}_{\rm r}-\dot{\phi}\in L_2\bigcap L_\infty \tag{28}$$

$$\dot{\phi}_{\rm d}-\dot{\phi}\in L_2\bigcap L_\infty \tag{29}$$

$$\phi_{\rm d}-\phi\in L_2\bigcap L_\infty \tag{30}$$

$$\tau_{\rm r}-\tau\in L_2\bigcap L_\infty. \tag{31}$$

Assume that the payload of the harmonic drive is governed by

$$m\ddot{q}+b\dot{q}+kq=\tau \tag{32}$$

where $m>0, b>0$, and $k\geq 0$. It follows that $\tau\in L_\infty$ in view of (31), and furthermore that $\dot{q}\in L_\infty$. Consequently, it yields $\dot{\phi}\in L_\infty$ in view of [23, Lemma 1, p. 1956] and (1). Thus, $\dot{\phi}_{\rm r}\in L_\infty$ is obtained. Finally, it follows that $Y_\phi(\dot{\phi}_{\rm r},\tau)(\theta-\hat{\theta})\in L_\infty$ and $[Y_\phi(\dot{\phi},\tau)-Y_\phi(\dot{\phi}_{\rm r},\tau)]\theta\in L_\infty$ in view of (3) and (4), and that $\ddot{\phi}_{\rm r}-\ddot{\phi}\in L_\infty$ in view of (18). Substituting (19) into (8), differentiating both sides with respect to time, and subtracting $\ddot{\phi}$ yields

$$\ddot{\phi}_{\rm r}-\ddot{\phi}=(1+k_{\rm f}\lambda_\tau d)(\ddot{\phi}_{\rm d}-\ddot{\phi})+(\lambda_\phi+k_{\rm f}\lambda_\tau)(\dot{\phi}_{\rm d}-\dot{\phi}) + k_{\rm f}\lambda_\tau\left[(\zeta-\hat{\zeta})\dot{\tau}_{\rm r}-\dot{\hat{\zeta}}\tau_{\rm r}\right].$$

It follows that $\ddot{\phi}_{\rm d}-\ddot{\phi}\in L_\infty$, in view of $\ddot{\phi}_{\rm r}-\ddot{\phi}\in L_\infty$, (29), $\tau_{\rm r}\in L_\infty, \dot{\tau}_{\rm r}\in L_\infty$, and $|\dot{\hat{\zeta}}|\leq \rho_\zeta\mid s_\zeta(t)\mid$. The asymptotic stability of

$$\dot{\phi}_{\rm r}-\dot{\phi}\to 0 \tag{33}$$

$$\dot{\phi}_{\rm d}-\dot{\phi}\to 0 \tag{34}$$

$$\phi_{\rm d}-\phi\to 0 \tag{35}$$

$$\tau_{\rm r}-\tau\to 0 \tag{36}$$

is therefore achieved [22]. Alternatively, $\tau_{\rm r}$ can be designed as

$$\tau_{\rm r}=\tau_{\rm d}+\lambda_{\rm f}\int_0^t(\tau_{\rm d}-\tau)dt \tag{37}$$

aimed at achieving accurate torque control $\tau_{\rm d}-\tau$ at low frequencies, where $\lambda_{\rm f}>0$ is a constant and $\tau_{\rm d}$ denotes the desired torque.

The results in the joint torque control mode can be summarized in the form of a theorem as follows.

Theorem 1: Consider a harmonic drive described by (1)–(4) combined with the adaptive control algorithms described by (5)–(14) subject to $\lambda_{\rm q}=0$ and (22). It follows that:

1) the L_2 stability from $u_{\rm d}$ to $\dot{\phi}_{\rm r}-\dot{\phi}, \phi_{\rm d}-\phi, \dot{\phi}_{\rm d}-\dot{\phi}$, and $\tau_{\rm r}-\tau$ in the sense of (23)–(26) can be achieved;
2) the L_∞ stability for $\dot{\phi}_{\rm r}-\dot{\phi}, \phi_{\rm d}-\phi, \dot{\phi}_{\rm d}-\dot{\phi}$, and $\tau_{\rm r}-\tau$ can be achieved, if $\tau_{\rm r}\in L_\infty$;
3) (28)–(31) are valid, if $u_{\rm d}\in L_2$ and $\tau_{\rm r}\in L_\infty$;
4) (33)–(36) are valid, if $u_{\rm d}\in L_2, \tau_{\rm r}\in L_\infty, \dot{\tau}_{\rm r}\in L_\infty$, and (32) holds.

C. Joint Position Control

In the position-control mode, the term $-(1+k_\tau)\lambda_{\rm q}(\dot{q}_{\rm r}-\dot{q})(\tau_{\rm r}-\tau)$ in (21) uniquely characterizes the dynamic coupling between the harmonic drive and its payload (the rest of the robot). This term allows the motion control to be carried out at the joints. Design

$$\tau_{\rm r}=\tau_{\rm d}+k_{\rm p}(\dot{q}_{\rm r}-\dot{q})+t_{\rm s} \tag{38}$$

$$t_{\rm s}=\mathcal{P}(\dot{q}_{\rm r}-\dot{q},k_{\rm I},t_{\rm s}^-,t_{\rm s}^+) \tag{39}$$

where $\tau_{\rm d}$ represents the desired torque computed from a motion controller, such as $Z_j^{T\,L_j}F_{\rm r}$ in [5]; $k_{\rm p}>0$ and $k_{\rm I}>0$ are two gains, and $t_{\rm s}^-<0$ and $t_{\rm s}^+>0$ are two constants. The term $t_{\rm s}$ acts as a bounded integral control of $\dot{q}_{\rm r}-\dot{q}$. The desired torque $\tau_{\rm d}$ takes a form as

$$\tau_{\rm d}=\tau_{\rm d}(\varrho,\underline{q},\dot{\underline{q}}) \tag{40}$$

$$\|\varrho\|\in L_\infty \tag{41}$$

$$\|\dot{\varrho}\|\in L_\infty \tag{42}$$

where ϱ denotes a vector characterizing the desired trajectories, and $\underline{q}$ denotes the joint coordinates (positions) of the entire robot. Equations (38)–(42) confirm Remark 3.3 in a sense that $\tau_{\rm r}$ and $\dot{\tau}_{\rm r}$ are functions of the referenced signals and of the positions, velocities, and accelerations of the entire robot.

Based on the definition of the $\mathcal{P}$ function in [5, p. 311], it can be verified that

$$-t_{\rm s}\left[(\dot{q}_{\rm r}-\dot{q})-\frac{\dot{t}_{\rm s}}{k_I}\right]\leq 0. \tag{43}$$

The second nonnegative function is defined as

$$V_2=\frac{1}{2}\frac{t_{\rm s}^2}{k_{\rm I}}. \tag{44}$$

It follows from (38)–(44) that

$$-(\dot{q}_{\rm r}-\dot{q})(\tau_{\rm r}-\tau)+\dot{V}_2\leq -k_{\rm p}(\dot{q}_{\rm r}-\dot{q})^2-(\dot{q}_{\rm r}-\dot{q})(\tau_{\rm d}-\tau). \tag{45}$$

It is important to note that the term $-(\dot{q}_{\rm r}-\dot{q})(\tau_{\rm d}-\tau)$ in (45) is exactly the same as $-(\dot{q}_{j\rm r}-\dot{q}_j)Z_j^T({}^{L_j}F_{\rm r}-{}^{L_j}F)=W_{T_j}-W_{L_j}$ appearing in [5, eq. (30)] or [24, eq. (B5)]. This represents the *virtual power flows* [5] at the two cutting points at which the harmonic drive is connected to a robotic system. This term is technically needed to cancel the virtual power flows of the rest of the robot[1]. Finally, a nonnegative function for the entire robotic system is chosen as

$$V=V_1+(1+k_\tau)\lambda_{\rm q}V_2+(1+k_\tau)\lambda_{\rm q}V_{\rm s} \tag{46}$$

[1]The two virtual power flows associated with the two neighbor subsystems at a common cutting point have the same magnitudes but with different signs.

where $V_{\rm s} \geq 0$ represents the summation of all the nonnegative accompanying functions assigned to the other subsystems (except for the harmonic drive itself), and possesses a form as

$$V_{\rm s} = \frac{1}{2}\tilde{\boldsymbol{X}}^T P \tilde{\boldsymbol{X}} + \alpha_{\rm s}(t) \tag{47}$$

where $\alpha_{\rm s}(t) \in L_\infty$ is a nonnegative function associated with the parameter errors and other bounded errors such as the quaternion; the vector $\tilde{\boldsymbol{X}}$ represents the state error of the rest of the robot, and P is a block diagonal positive-definite symmetric matrix. Since all the virtual power flows inside the system will be canceled out [4], [5], [24], it yields

$$\begin{aligned}\dot{V} \leq (\gamma u_{\rm d})^2 - \left[k_\phi - \left(\frac{1}{2\gamma}\right)^2\right](\dot{\phi}_{\rm r} - \dot{\phi})^2 \\ - (1+k_\tau)k_{\rm f} d(\dot{\phi}_{\rm d} - \dot{\phi})^2 - (1+k_\tau)k_{\rm f}\lambda_\phi(\phi_{\rm d} - \phi)^2 \\ - (1+k_\tau)\lambda_\tau(\tau_{\rm r} - \tau)^2 - (1+k_\tau)\lambda_{\rm q}k_{\rm p}(\dot{q}_{\rm r} - \dot{q})^2 \\ - (1+k_\tau)\lambda_{\rm q}V_{\rm s}^*\end{aligned} \tag{48}$$

where

$$V_{\rm s}^* = \tilde{X}^T Q \tilde{X} \tag{49}$$

and Q represents a block diagonal positive-definite symmetric matrix. By specifying $\gamma^2 = \frac{1}{2k_\phi}$, integrating (48) over time from $t = 0$ to $t = T, \forall\, T > 0$, yields

$$\begin{aligned}\int_0^T (\dot{q}_{\rm r} - \dot{q})^2 dt \leq \frac{1}{2k_\phi(1+k_\tau)\lambda_{\rm q}k_p}\int_0^T u_{\rm d}^2 dt \\ + \frac{1}{(1+k_\tau)\lambda_{\rm q}k_p}V(0)\end{aligned} \tag{50}$$

together with (23)–(26) by substituting $V(0)$ for $V_1(0)$. This results in the L_2 stability from $u_{\rm d}$ to $\dot{\phi}_{\rm r} - \dot{\phi}, \phi_{\rm d} - \phi, \dot{\phi}_{\rm d} - \dot{\phi}, \tau_{\rm r} - \tau$, and $\dot{q}_{\rm r} - \dot{q}$. If $u_{\rm d} \in L_2$, it follows that $\dot{\phi}_{\rm r} - \dot{\phi} \in L_2, \phi_{\rm d} - \phi \in L_2, \dot{\phi}_{\rm d} - \dot{\phi} \in L_2, \tau_{\rm r} - \tau \in L_2$, and $\dot{q}_{\rm r} - \dot{q} \in L_2$. In view of (46), (48), and Lemma 1, it follows that $\tilde{\boldsymbol{X}} \in L_\infty$. If the joint velocity error is limited by the state error of the rest of the robot,[2] i.e.,

$$|\, \dot{q}_{\rm r} - \dot{q} \,| \leq c_{\rm v}\|\tilde{\boldsymbol{X}}\| \tag{51}$$

with $c_{\rm v} > 0$, it yields

$$\dot{q}_{\rm r} - \dot{q} \in L_2 \bigcap L_\infty \tag{52}$$

in addition to (28) and (30). Once the required joint velocity $\dot{q}_{\rm r}$ is designated as

$$\dot{q}_{\rm r} = \dot{q}_{\rm d} + \lambda(q_{\rm d} - q) \tag{53}$$

where $q_{\rm d}$ is the desired joint position, and $\lambda > 0$ is a control parameter that is analogous to the eigenvalue of a sliding surface in variable structure control, it immediately follows from [23, Lemma 1, p. 1956] that

$$\dot{q}_{\rm d} - \dot{q} \in L_2 \bigcap L_\infty \tag{54}$$

$$q_{\rm d} - q \in L_2 \bigcap L_\infty. \tag{55}$$

[2]This case is true in [4], [5], and [24].

Assume that $q_{\rm d} \in L_\infty, \dot{q}_{\rm d} \in L_\infty, \ddot{q}_{\rm d} \in L_\infty$, and $q_{\rm d}^{(3)} \in L_\infty$. It yields $q \in L_\infty$ and $\dot{q} \in L_\infty$ from (54) and (55). If the proposed joint control law is extended to all the joints such that

$$q \in L_\infty \Rightarrow \underline{q} \in L_\infty \tag{56}$$

$$\dot{q} \in L_\infty \Rightarrow \underline{\dot{q}} \in L_\infty \tag{57}$$

it follows from (40) and (41) that $\tau_{\rm d} \in L_\infty$. Furthermore, it follows from (38), (39), and (52) that $\tau_{\rm r} \in L_\infty$.

In view of (8) and (19), it yields

$$\begin{bmatrix} 1 & \lambda_\tau \\ -k_{\rm f}d & 1 \end{bmatrix}\begin{bmatrix} \dot{\phi}_{\rm d} - \dot{\phi} \\ \tau_{\rm r} - \tau \end{bmatrix} = \begin{bmatrix} \dot{\phi}_{\rm r} - \dot{\phi} - \lambda_\phi(\phi_{\rm d} - \phi) - \lambda_{\rm q}(\dot{q}_{\rm r} - \dot{q}) \\ k_{\rm f}(\phi_{\rm d} - \phi) + k_{\rm f}\tau_{\rm r}(\zeta - \hat{\zeta}) \end{bmatrix}. \tag{58}$$

for a nonzero $\lambda_{\rm q}$. It follows from (28), (30), (52), and $\tau_{\rm r} \in L_\infty$ that

$$\dot{\phi}_{\rm d} - \dot{\phi} \in L_\infty \tag{59}$$

$$\tau_{\rm r} - \tau \in L_\infty. \tag{60}$$

Consequently, it yields $\tau \in L_\infty$ from (60).

Let $\underline{\tau}$ be the joint-torque vector of the entire robot. If the proposed joint control law is extended to all the joints such that

$$\tau \in L_\infty \Rightarrow \underline{\tau} \in L_\infty \tag{61}$$

then the boundedness of joint accelerations

$$\ddot{q} \in L_\infty \tag{62}$$

$$\underline{\ddot{q}} \in L_\infty \tag{63}$$

can be ensured in terms of the robot dynamics nature characterized by

$$\|\underline{\ddot{q}}\| \leq c_{\rm a}\|\underline{\tau}\| + \varepsilon(t) \tag{64}$$

where $c_{\rm a} > 0, \varepsilon(t) \geq 0$, and $\varepsilon(t) \in L_\infty$. It further guarantees $\dot{\tau}_{\rm d} \in L_\infty$ from the time derivative of (40) and (42). Note that $\tau \in L_\infty$ implies $\dot{\phi} \in L_\infty$ in view of (1) and [23, Lemma 1, p. 1956] and further implies $\dot{\phi}_{\rm r} \in L_\infty$ in view of (28).

Under $\tau \in L_\infty, \dot{\phi} \in L_\infty$, and $\dot{\phi}_{\rm r} \in L_\infty$, (3) implies

$$[Y_\phi(\dot{\phi}, \tau) - Y_\phi(\dot{\phi}_{\rm r}, \tau)]\theta \in L_\infty \tag{65}$$

$$Y_\phi(\dot{\phi}_{\rm r}, \tau)(\theta - \hat{\theta}) \in L_\infty. \tag{66}$$

Thus, it yields $\ddot{\phi}_{\rm r} - \ddot{\phi} \in L_\infty$ in view of (18), (28), (60), (65), and (66). Furthermore, it yields $\ddot{q}_{\rm r} - \ddot{q} \in L_\infty$ in view of the time derivative of (53), (54), and (62). It follows from $\dot{\tau}_{\rm d} \in L_\infty$, the time derivatives of (38) and (39), and (52) that $\dot{\tau}_{\rm r} \in L_\infty$. Finally, it yields $\ddot{\phi}_{\rm d} - \ddot{\phi} \in L_\infty$ and $\dot{\tau}_{\rm r} - \dot{\tau} \in L_\infty$ in view of the time derivatives of (12) and (58), and (14), (30), (59), $\tau_{\rm r} \in L_\infty$, and $\dot{\tau}_{\rm r} \in L_\infty$. Therefore, the asymptotic stability of

$$\dot{q}_{\rm r} - \dot{q} \to 0 \tag{67}$$

$$\dot{q}_{\rm d} - \dot{q} \to 0 \tag{68}$$

$$q_{\rm d} - q \to 0 \tag{69}$$

can be achieved in addition to (33)–(36) [22].

The results obtained in the joint position control mode can be summarized in the form of a theorem as follows.

Theorem 2: Consider a harmonic drive described by (1)–(4) combined with the adaptive-control algorithms described by (5)–(14), (38), (39), and (53), subject to (22), (40)–(42), (47), and (49). It follows that

1) the L_2 stability from $u_{\rm d}$ to $\dot{\phi}_{\rm r}-\dot{\phi}, \phi_{\rm d}-\phi, \dot{\phi}_{\rm d}-\dot{\phi}, \tau_{\rm r}-\tau$, and $\dot{q}_{\rm r}-\dot{q}$ can be achieved;
2) the L_∞ stability for $\dot{\phi}_{\rm r}-\dot{\phi}, \phi_{\rm d}-\phi, \dot{\phi}_{\rm d}-\dot{\phi}, \tau_{\rm r}-\tau$, and $\dot{q}_{\rm r}-\dot{q}$ can be achieved, if $q_{\rm d}\in L_\infty, \dot{q}_{\rm d}\in L_\infty, \ddot{q}_{\rm d}\in L_\infty$, and (51), (56), and (57) hold;
3) (28)–(31), (52), (54), and (55) are valid, if $q_{\rm d}\in L_\infty, \dot{q}_{\rm d}\in L_\infty, \ddot{q}_{\rm d}\in L_\infty, u_{\rm d}\in L_2$, and (51), (56), and (57) hold;
4) (33)–(36) and (67)–(69) are valid, if $q_{\rm d}\in L_\infty, \dot{q}_{\rm d}\in L_\infty, \ddot{q}_{\rm d}\in L_\infty, q_{\rm d}^{(3)}\in L_\infty, u_{\rm d}\in L_2$, and (51), (56), (57), (61), and (64) hold.

IV. Experiments

Four types of harmonic drives as listed in Table I are tested with the proposed control approach. Each harmonic drive is equipped with a resolver at the joint, an encoder at the motor, and four pairs of strain gauges placed at the flexspline, based on the guidelines in [15]. The four types of harmonic drives are located at joints 3, 4, 5, and 7 of a seven-joint redundant robot manipulator associated with the CSA automation and robotics testbed (CART).

The QNX-based real-time operating system with RT-LAB from OPAL-RT is adopted as a main platform for control computation with a sampling rate of 1000 Hz.

The control parameters for all the four joints associated with different types of harmonic drives are listed in Table II in which three groups of parameters are presented. The first seven rows correspond to the control parameters in (5)–(9); the next 15 rows correspond to the parameter adaptation laws (11) and (12); and the last five rows correspond to the joint motion controller specified by (38), (39), and (53).

In view of Remark 3.3, the variables required for implementing the control torque u include $q, \dot{q}, \ddot{q}, \phi, \dot{\phi}, \tau$, and $\dot{\tau}$. In the implementation, only q, ϕ, and τ are taken directly from the measurements. The remaining variables $\dot{q}, \ddot{q}, \dot{\phi}$, and $\dot{\tau}$ are generated numerically by using $s \Rightarrow s\frac{200}{s+200} \Rightarrow \frac{200(z-1)}{z-0.8}$, where a low-pass filter with a cutoff frequency of $200\,{\rm rad/s}$ is added and $s=\frac{z-1}{T}$ with $T=0.001\,{\rm s}$ is applied. For joint 7, the resolver gives a $2\pi/2^{16}\approx 9.6\times 10^{-5}\,{\rm rad}$ resolution for q, which is equivalent to a $9.6\times 10^{-5}\times 200^2\approx 3.8\,{\rm rad/s^2}$ resolution for $\ddot{q}$. In view of $I^*=1.0\,{\rm N\cdot m\cdot s^2}$, it yields a 3.8-N·m torque resolution for the control. The maximum continuous torques for joint 7 is $0.63\times 160=100.8$ N·m. Thus, the numerical-differentiation-induced torque ripple takes less than 4% of the maximum continuous control torque. On the other hand, the use of the derivative of the measured torque will introduce $I^*\lambda_\tau\times 200\approx 0.04$ times torque measurement noise into the control torque for joint 7. The same analysis applies to the other three joints. In summary, the use of high-order time derivatives of the measurement variables through numerical differentiation only introduces an acceptable level of noise to the control torque.

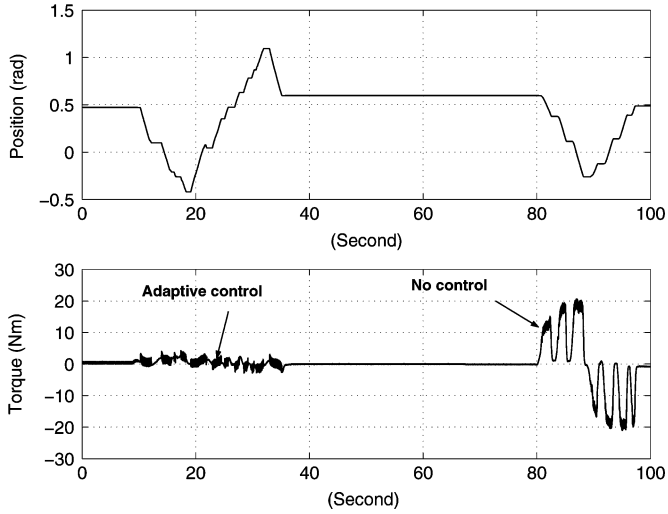

Fig. 2. Backdrive ability with and without control.

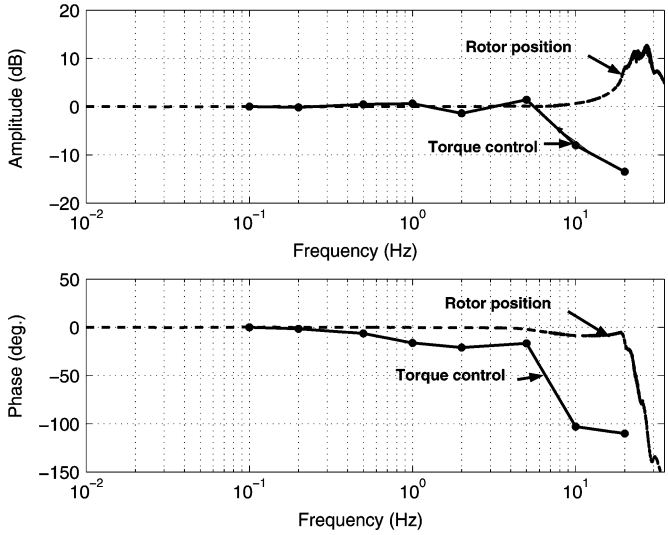

Fig. 3. Transfer functions of the joint torque control. The dashed lines represent the motor rotor position control transfer function $\phi/\phi_{\rm d}$, and the solid lines represent the torque control transfer function $\tau/\tau_{\rm r}$.

To demonstrate the effectiveness of the proposed control approach, both joint torque control and joint position control are tested.

In the joint torque control mode, the experimental results are illustrated in Figs. 2–4. In Fig. 2, the effectiveness of the torque control is verified by testing the backdrive ability of the harmonic drive in joint 7, i.e., under zero torque command $(\tau_{\rm r}=0)$, the harmonic drive is back driven by hand from the output axis. The upper plot shows the position and the lower plot shows the joint torque. The first experiment between 0 and 40 s is conducted with the proposed adaptive controller activated under $\tau_{\rm r}=0$. The second experiment between 80 and 100 s is conducted without the control. It can be clearly seen that the backdrive ability is substantially improved by using the proposed adaptive controller in the joint torque control mode. For

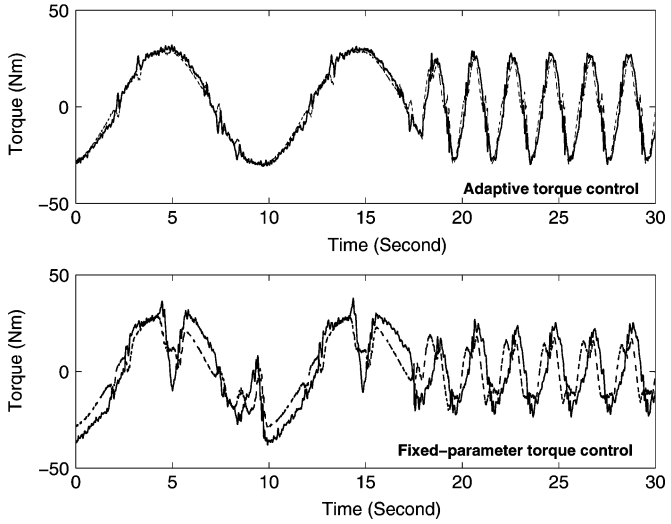

Fig. 4. Comparison of the adaptive friction compensation (*top*) with the fixed-parameter friction compensation (*bottom*). The dashed lines represent the required torques ($\tau_{\rm r}$) and the solid lines represent the actual torques (τ).

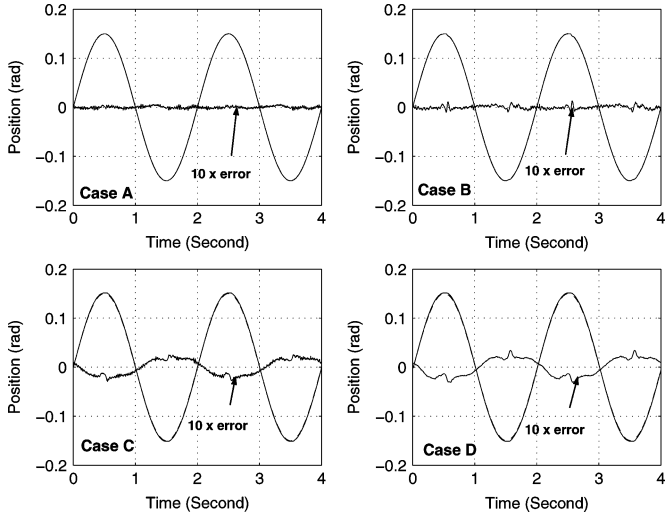

Fig. 5. Position tracking control under a 0.5-Hz sinusoidal input in four cases. *Case A:* the proposed control. *Case B:* adaptive friction compensation only. *Case C:* flexspline dynamics only. *Case D:* PID control. The dashed lines represent the desired positions and the solid lines represent the actual positions. In each subplot, an additional curve representing ten times the position tracking error is also illustrated.

similar movements, the hand (external) driving torque becomes much smaller.

Fig. 3 shows the transfer functions[3] of the joint torque tracking control $\tau/\tau_{\rm r}$ and the corresponding motor rotor position tracking control $\phi/\phi_{\rm d}$ of joint 7. The joint torque tracking control performs well until 6 Hz. The motor rotor position tracking control performs well until 10 Hz. The overshoot in the transfer function $\phi/\phi_{\rm d}$ around 25 Hz is mainly due to the distributed parameter dynamics that governs the resonant modes of the flexspline.

Fig. 4 shows the effectiveness of the adaptive friction compensation (top) versus the fixed-parameter friction compensation (bottom) of joint 3. It can be clearly seen that with adaptive friction compensation, the tracking performance is obviously superior.

In the joint position control mode, the experimental results are illustrated in Figs. 5–8. Experiments start with joint 7. Four cases, namely A–D, are tested separately to demonstrate the effectiveness of each control design. Case A represents the use of the proposed adaptive controller; case B represents the use of the adaptive friction compensation only, without using the flexspline dynamics, typically by setting $I^* = 0, k_\phi = 0, \lambda_{\rm q} = 0, \lambda_\tau = 0, k_\tau = 0$, and $\phi_{\rm d} = \phi$; case C represents the use of the flexspline-dynamics-based control only, without using the adaptive friction compensation, typically by setting $\hat{f}_\phi(\dot{\phi}_{\rm r}) = 0$ in (9); and case D represents a PID control in which neither the adaptive friction compensation nor the flexspline-dynamics-based control is used. Thus, the difference between cases A and D characterizes the feasibilities of the proposed control.

For joint 7, the position tracking control results in all four cases with respect to 0.5 and 5.0 Hz sinusoidal inputs are illustrated in Figs. 5 and 6, respectively, with the maximum tracking errors listed in Table III. An improvement of about four times in the position tracking control has been achieved by comparing case A with case D. Meanwhile, it has been shown that both the joint friction compensation and the flexspline-dynamics-based control provide significant improvements toward reducing tracking errors. Roughly speaking, the friction compensation makes more contributions at lower frequencies and the flexspline-dynamics-based control makes more contributions at higher frequencies. In Fig. 7, the transfer functions[4] of the joint

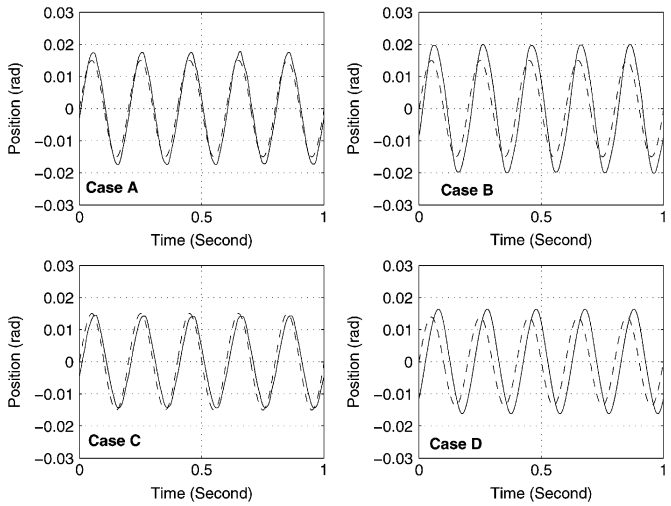

Fig. 6. Position tracking control under a 5.0-Hz sinusoidal input in four cases. *Case A:* the proposed control. *Case B:* adaptive friction compensation only. *Case C:* flexspline dynamics only. *Case D:* PID control. The dashed lines represent the desired positions and the solid lines represent the actual positions.

[3]The desired torque is a chirp signal of 8 $\rm N\cdot m$ varying from 0.01 to 10 Hz in 100 s. Meanwhile, sinusoidal signals of 2 N·m are added at 0.1, 0.2, 0.5, 1, 2, 5, 10, and 20 Hz to enhance the confidence.

[4]The desired position is a chirp signal of 0.2 $\rm rad/s$ varying from 0.01 to 10 Hz in 100 s, passing through an integrator.

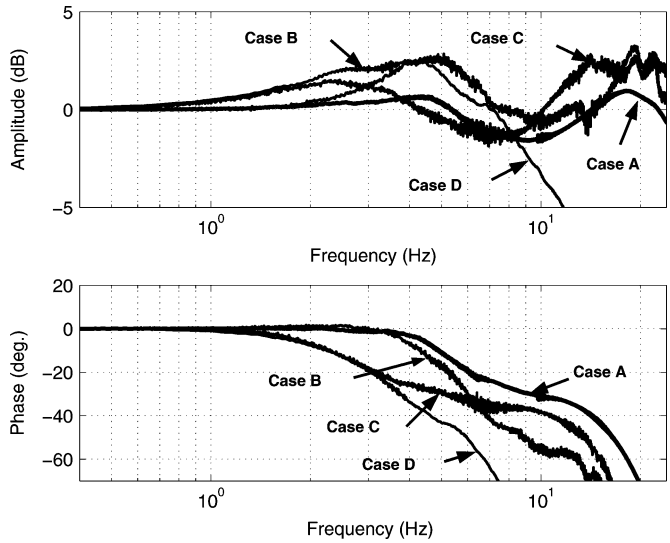

Fig. 7. Transfer functions of the joint position control $q/q_{\rm d}$ in four cases. *Case A:* the proposed control. *Case B:* adaptive friction compensation only. *Case C:* flexspline dynamics only. *Case D:* PID control.

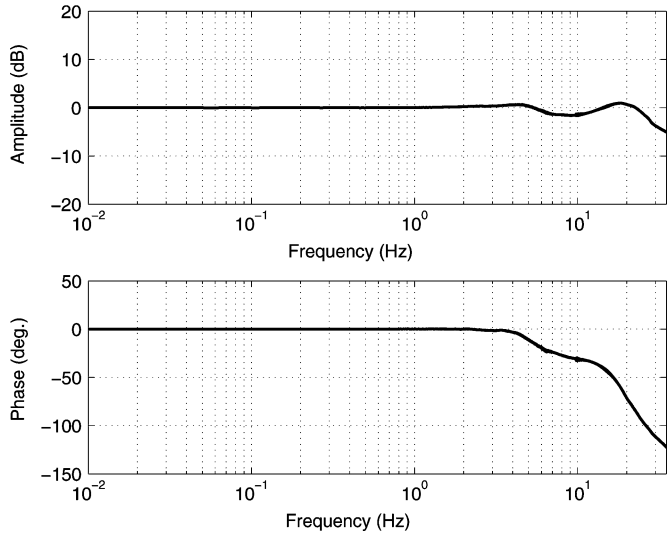

Fig. 8. Transfer function of the joint position control $q/q_{\rm d}$.

position tracking control of joint 7 in all four cases are plotted along most important frequencies. Case A gives the most flat transfer function around 0 dB with the least phase lag, case B possesses a 3-dB overshoot around 5 Hz and another overshoot after 14 Hz, case C has a large phase lag starting after 1 Hz, and case D takes the disadvantages of both cases B and C by having a 3-dB overshoot around 4.5 Hz and having a large phase lag starting after 1 Hz. The transfer function of case A along the complete frequency range is illustrated in Fig. 8. Compared to the result of the joint torque tracking control given in Fig. 3, the result of the joint position tracking control is much better. This can be partially explained by the fact that the imperfection of torque control is compensated somehow by the position feedback loop characterized by (38), (39), and (53).

TABLE III
MAXIMUM TRACKING ERRORS UNDER DIFFERENT SINUSOIDAL INPUTS

Frequency (Hz)	Amplitude (rad)	Maximum tracking errors e (rad)				$\frac{Max\|e\|}{Max\|v\|+0.2Max\|a\|}$	
		Case A	Case B	Case C	Case D	Case A	Case D
0.5	0.15	0.0008	0.00116	0.00295	0.0034	0.001	0.0044
5.0	0.015	0.0033	0.0088	0.005	0.0122	0.00096	0.0036

TABLE IV
CONTROL PERFORMANCE

	Frequency (Hz)	Amplitude (rad)	$Max \mid v \mid$ (rad/s)	$Max \mid a \mid$ (rad/s^2)	$Max \mid e \mid (rad)$	
					Case A	Case D
Joint 3	0.5	0.1	0.314	0.987	0.0004	0.0023
	2.0	0.02	0.251	3.158	0.0021	0.0052
Joint 4	0.5	0.1	0.314	0.987	0.0005	0.0030
	2.0	0.02	0.251	3.158	0.0020	0.0060
Joint 5	0.5	0.1	0.314	0.987	0.0006	0.0025
	2.0	0.02	0.251	3.158	0.0020	0.0040
Joint 7	0.5	0.15	0.471	1.48	0.0008	0.0034
	5.0	0.015	0.471	14.804	0.0033	0.0122

Generally speaking, a large tracking error is always associated with a large velocity and acceleration. In order to quantify the control performance of the proposed controller in a comparable common basis, an index

$$\frac{\max \mid q_{\rm d} - q \mid}{\max \mid \dot{q}_{\rm d} \mid + k(\max \mid \ddot{q}_{\rm d} \mid)} \tag{70}$$

where $k > 0$, is defined. Its values in cases A and D for joint 7 are listed in Table III.

By using the virtual decomposition control algorithms designed for controlling the robot linkage [5], the proposed joint adaptive controller has been tested on all four joints. The maximum joint tracking errors in cases A and D under different sinusoidal inputs for joints 3, 4, 5, and 7 are summarized in Table IV. Like the results for joint 7, the maximum joint position tracking errors for joints 3–5 have been reduced significantly.

V. CONCLUSION

With respect to the particular dynamics of harmonic drives, namely the high friction and the flexspline dynamics, an adaptive control algorithm has been developed and tested in both joint torque control and joint position control modes. The proposed controller guarantees the L_2 and L_∞ stability and the L_2-gain induced H_∞ stability. In view of the virtual decomposition control, the developed adaptive controller for harmonic drives can be efficiently incorporated into the robot motion control system, since the dynamic coupling between each joint equipped with a harmonic-motor pair and the rest of the robot is completely characterized by a scale term that is represented as a product of the joint velocity error and the torque error. The experimental results carried out with respect to the four different types of harmonic drives from HD Systems Inc. have demonstrated superior performance in both joint torque control and joint position control. The attempt to adaptively compensate for the friction and to take into account the flexspline dynamics have been proven to be effective.

REFERENCES

[1] M. C. Good, L. M. Sweet, and K. L. Strbel, "Dynamic models for control system design of integrated robot and drive systems," *ASME. J. Dyn. Syst. Meas. Control*, vol. 107, no. 1, pp. 53–59, Mar. 1985.

[2] I. Godler and M. Hashimoto, "Torque control of harmonic drive gears with built-in sensing," in *Proc. IECON'98*, 2006, vol. 3, pp. 1818–1823.

[3] P. S. Gandhi, F. H. Ghorbel, and J. Dabney, "Modeling, identification, and compensation of friction in harmonic drives," in *Proc. 41st IEEE Conf. Decision Control*, 2002, vol. 1, pp. 160–166.

[4] W.-H. Zhu, Y. G. Xi, Z. J. Zhang, Z. Bien, and J. De Schutter, "Virtual decomposition based control for generalized high dimensional robotic systems with complicated structure," *IEEE Trans. Robot. Autom.*, vol. 13, no. 3, pp. 411–436, Jun. 1997.

[5] W.-H. Zhu and J. De Schutter, "Adaptive control of mixed rigid/flexible joint robot manipulators based on virtual decomposition," *IEEE Trans. Robot. Autom.*, vol. 15, no. 2, pp. 310–317, Apr. 1999.

[6] T. D. Tuttle and W. P. Seering, "A nonlinear model of a harmonic drive gear transmission," *IEEE Trans. Robot. Autom.*, vol. 12, no. 3, pp. 368–374, Jun. 1996.

[7] N. M. Kircanski and A. A. Goldenberg, "An experimental study of nonlinear stiffness, hysteresis, and friction effects in robot joints with harmonic drives and torque sensors," *Int. J. Robot. Res.*, vol. 16, no. 2, pp. 214–239, 1997.

[8] R. Dhaouadi, F. H. Ghorbel, and P. S. Gandhi, "A new dynamic model of hysteresis in harmonic drives," *IEEE Trans. Ind. Electron.*, vol. 50, no. 6, pp. 1165–1171, Dec. 2003.

[9] H. Kazerooni, "Dynamics and control of instrumented harmonic drives," *ASME J. Dyn. Syst. Meas. Control*, vol. 117, no. 1, pp. 15–19, 1995.

[10] H. D. Taghirad and P. R. Belanger, "H_∞-based robust torque control of harmonic drive systems," *ASME. J. Dyn. Syst. Meas. Control*, vol. 123, no. 3, pp. 338–345, 2001.

[11] G. Zhang and J. Furusho, "Control of robot arms using joint torque sensor," *IEEE Control Syst. Mag.*, vol. 18, no. 1, pp. 48–55, Feb. 1998.

[12] M. W. Spong, "Modeling and control of elastic joint robots," *ASME. J. Dyn. Syst. Meas. Control*, vol. 109, pp. 310–319, 1987.

[13] M. Hashimoto, "Robot motion control based on joint torque sensing," in *Proc. 1989 IEEE Int. Conf. Robot. Autom.*, pp. 256–261.

[14] K. Kosuge, H. Takeuchi, and K. Furuta, "Motion control of a robot arm using joint torque sensors," *IEEE Trans. Robot. Autom.*, vol. 6, no. 2, pp. 258–263, Apr. 1990.

[15] M. Hashimoto, Y. Kiyosawa, and R. P. Paul, "A torque sensing technique for robots with harmonic drives," *IEEE Trans. Robot. Autom.*, vol. 9, no. 1, pp. 108–116, Feb. 1993.

[16] I. Godler, M. Horiuchi, M. Hashimoto, and T. Ninomiya, "Accuracy improvement of built-in torque sensing for harmonic drives," *IEEE/ASME Trans. Mechatronics*, vol. 5, no. 4, pp. 360–366, Dec. 2000.

[17] H. K. Khalil, *Nonlinear Systems*, 2nd ed. Englewood Cliffs, NJ: Prentice-Hall, 1996.

[18] A. J. van der Schaft, "L_2-gain analysis of nonlinear systems and nonlinear state feedback H_∞ control," *IEEE Trans. Autom. Control*, vol. 37, no. 6, pp. 770–784, Jun. 1992.

[19] A. Albu-Schaffer and G. Hirzinger, "Parameter identification and passivity based joint control for a 7 DOF torque controlled light weight robot," in *Proc. 2001 IEEE Int. Conf. Robot. Autom.*, Seoul, Korea, May 2001, pp. 2852–2858.

[20] A. De Luca, R. Farina, and P. Lucibello, "On the control of robots with visco-elastic joints," in *Proc. 2005 IEEE Int. Conf. Robot. Autom.*, Barcelona, Spain, Apr. 2001, pp. 4308–4313.

[21] R. Lozano and B. Brogliato, "Adaptive control of robot manipulators with flexible joints," *IEEE Trans. Autom. Control*, vol. 37, no. 2, pp. 174–181, Feb. 1992.

[22] G. Tao, "A simple alternative to the Barbălat lemma," *IEEE Trans. Autom. Control*, vol. 42, no. 5, p. 698, May 1997.

[23] W.-H. Zhu and S. E. Salcudean, "Stability guaranteed teleoperation: An adaptive motion/force control approach," *IEEE Trans. Autom. Control*, vol. 45, no. 11, pp. 1951–1969, Nov. 2000.

[24] W.-H. Zhu, Z. Bien, and J. De Schutter, "Adaptive motion/force control of multiple manipulators with joint flexibility based on virtual decomposition," *IEEE Trans. Autom. Control*, vol. 43, no. 1, pp. 46–60, Jan. 1998.

Wen-Hong Zhu (M'97–SM'05) received the Bachelor's and the M.S. degrees, both in aeronautical control engineering, from the Northwestern Polytechnic University, Xi'an, China, in 1984 and 1987, respectively. He received the Ph.D. degree in information and control engineering from Xi'an Jiaotong University, Xi'an, China, in 1991.

In 1995, he was a Postdoctoral Fellow with CIET, KAIST, Korea. During 1996–1997, he was a Postdoctoral Fellow in the Katholieke Universiteit Leuven, Belgium. From 1997 to 2001, he was a Post doctoral Fellow/Scientific Engineer at the University of British Columbia, BC Canada. Since 2001, he has been an Engineer with the Canadian Space Agency, Saint-Hubert, QC, Canada. His previous research has been concerned with the development of the virtual decomposition control (VDC) approach capable of handling the adaptive control problem of complex robots by solely using subsystem dynamics while guaranteeing the stability and convergence of the entire system. He has successfully applied the VDC approach to coordinated control of multiple robots, force control with rigid contact, and adaptive teleoperation control with guaranteed stability. His current research interests include adaptive control of harmonic drives, adaptive joint force/torque control of hydroulic robots, control of high-speed feed drives, high-precision control of piezoactuators, active control of microgravity isolation systems, teleoperated control of medical robots, variable structure control of robots with joint position measurements, and application of robots in service fields.

Dr. Zhu was the recipient of the Swedish Open Championship in Robust Robot Control, sponsored by ABB, in 2004.

Erick Dupuis received the B.Sc.A. from the University of Ottawa, Ottawa, ON, Canada, in 1990, the Master's degree from the Massachusetts Institute of Technology, Cambridge, in 1992, and the Ph.D. degree from McGill University, Montreal, QC, Canada, in 2001, all in mechanical engineering.

In 1992, he joined the Canadian Space Agency, Saint-Hubert, QC, Canada, as a Robotics Research Engineer. During 1997–2001, he was also a Systems Engineer for the SPDM Task Verification Facility. He has also been the Lead Engineer for the Canadian Space Agency's space exploration activities. His previous research has been concerned with the control of space robots from the ground. Since 2002, he has been the Manager of the Robotics Group with the Space Technologies Branch, Canadian Space Agency. His current research activities focus on the development of autonomy software for space robots in planetary exploration and on-servicing applications.

Michel Doyon received the Bachelor's degree in electrical engineering from Laval University, Quebec City, QC, Canada, in 1992, and the Master's degree in robotics from McGill University, Montreal, QC, Canada, in 1994.

He is currently the Acting Program Manager for Space Science and Exploration with the Space Technologies Branch, Canadian Space Agency, Saint-Hubert, QC, Canada. His previous research interests include robotics, simulations, and real-time control systems. Currently, he is in-charge of the planning and funding of the contracted-out Technology Research and Development activities in the field of space science and exploration.

Jean-Claude Piedboeuf received the Graduate degree in mechanical engineering, and the Msc.A. and the Ph.D. degrees, both in electrical engineering, all from École Polytechnique, Montrial, QC, Canada, in 1983, 1985, and 1989, respectively.

During 1989–1990, he was with the Technical Institute of Munich, Munich, Germany. During 1990–1995, he was an Assistant Professor and then an Associate Professor in the Mechanical Engineering Department, Royal Military College of Canada, Kingston, ON, Canada. In 1996, he joined the Canadian Space Agency (CSA), Saint-Hubert, QC, Canada as a Researcher in dynamics. In 1997, he was a Manager of the Robotics section in the Spacecraft Engineering Directorate of the Space Technologies Branch of the CSA. In May 2002, he was the Deputy Director of the Spacecraft Engineering Directorate. In December 2003, he was an Advisor in Sciences and Technologies to the Vice-President Sciences, Technologies, and Programs. During 2004–2005, he was the Acting Director for the Directorate of Technology Management and Applications in the Space Technologies Branch. During 2001–2004, he was the Coordinator of the Space Technology Research Program that covers all the internal and collaborative research and developmental activities in Space Technologies. He is also an Associate Professor in the Department of Electrical Engineering at the École Polytechnique, and in the Department of System Engineering at the University of Waterloo, Waterloo, ON, Canada.

Dr. Piedboeuf was the Chair of i-SAIRAS 2001 and is also on its Organizing Committee. He was the Co-chair of the On-Orbit Servicing (OOS) 2002 Workshop, Germany, and the Local Chair for OOS 2004, Vancouver.